FUDMA Journal of Engineering and Technology
ISSN: 3092-9385
https://fjet.fudutsinma.edu.ng/index.php/fjet/
Volume 2, Issue 1, 2026, 547-559

Adaptive Hybrid Compliant Control of a Desktop Upper-Limb Rehabilitation Robot

Auwalu M. ABDULLAHI[1], Musa M. BELLO[2*], Ado HARUNA[3], Amina I. KHALEEL[4], Lubabatu B. ILA[5], Abdurrahaman M. BELLO[6]

[1,2*,4,5,6]Department of Mechatronics Engineering, Bayero University Kano, Nigeria.
[3]Department of Control and Mechatronics Engineering, Universiti Teknologi Malaysia

[1]amabdullahi.mct@buk.edu.ng, [2*]mbmusa.mct@buk.edu.ng, [3]aharuna.mct@buk.edu.ng, [4]aikhaleel.mct@buk.edu.ng, [5]lbila.mct@buk.edu.ng, [6]ambello.mct@buk.edu.ng

Abstract

Robotic rehabilitation systems, including exoskeletons and endpoint robots, are increasingly employed in physiotherapy for patients recovering from spinal cord injuries and stroke. Conventional rehabilitation relies heavily on physiotherapists and hospital-based sessions, which often involve scheduling constraints and long waiting times due to the high number of patients. Robotic assistance can alleviate this burden by enabling more frequent and consistent therapy while maintaining safe and effective human–robot interaction. Achieving safe interaction requires compliant control strategies capable of regulating the contact force between the patient and the robot, particularly in rehabilitation scenarios involving uncertain environments where interaction dynamics vary depending on soft or stiff contact conditions. Hybrid impedance and admittance position control (HIPC) has been widely adopted for this purpose. However, conventional HIPC typically employs fixed impedance parameters, which may lead to excessive energy consumption and reduced adaptability during therapy. This paper proposes a Hybrid Adaptive Impedance and Position Control (HAIPC) framework for robot-assisted rehabilitation. The proposed approach integrates a genetic algorithm–tuned PD-based admittance position controller for trajectory guidance with an adaptive impedance controller that dynamically updates stiffness and damping gains. An extended state observer is employed to estimate the contact torque, enabling adaptive control without the need for torque/force sensors. Simulation results demonstrated that the proposed HAIPC significantly reduces energy consumption by about 64% and reduces the contact torque tracking error to a similar extent compared to the conventional HIPC. The proposed strategy improves adaptability during human–robot interaction while offering a cost-effective sensorless implementation for rehabilitation robots.

Keywords: *Adaptive impedance control, Contact force estimation, Hybrid control, Upper-limb robot.*

1.0 Introduction

Impedance control was first introduced by Hogan in [1, 2], the idea was based on safety and stability provided by this type of control during robot interaction with its environment. There are two main types of interaction control widely used; the impedance and admittance controls. In impedance control the input is either position or velocity and the output is force, while admittance is opposite of the impedance control where the input is force and the output is either position or velocity [3]. When robot makes contact with an environment, there is need to control both the contact force and its motion. Generally, impedance control is more stable as compared to admittance control if the environment is stiff, while the admittance control is more suitable when the robot interacts with soft environments. Thus, when a robot interacts with an unknown environment, the choice of either impedance or admittance becomes a difficult task. Therefore, a combined impedance and admittance was proposed in [4] in which the two controllers are connected in parallel via a switch. The switching occurs based on the nature of the environment. Therefore, a hybrid impedance control was used in combining the two fundamental force controls to simultaneously control both position/force control and impedance control [5].

Recently, hybrid impedance control has been designed and implemented on various rehabilitation robotic arms and industrial robots to enhance safety and stability. Hybrid impedance control was first introduced in [5], in which position/force control and impedance control are combined and implemented within a single framework. The implementation is conducted by splitting the two controllers into two subspaces. Therefore, the position and force are commanded and controlled along different subspace. A robust hybrid impedance control was proposed in [6-7]. A hybrid impedance control was proposed by [8], the proposed controller concurrently realizes position motion tracking for rehabilitation and generate a force using optimization process based on a musculoskeletal model-based. Several other hybrid impedance control methods are presented in [9-11].

Impedance control regulates contact force to achieve robot compliance with different types of environmental property. However, the magnitude of contact force is unknown and its value depends on the inertia, damping and stiffness of the environment. In most cases, the actual values of inertia, damping and stiffness are difficult to find, therefore, the magnitude of contact force is estimated. Several methods have been proposed for estimation of

Received: 26/03/2026; Revised: 20/04/2026; Accepted: 21/04/2026; Published: 25/04/2026

contact force such as extended Kalman filter proposed in [12] for contact force/torque estimation of six-degree-of-freedom robot. Recently, an adaptive Kalman filter was proposed in [13] to estimated contact force in serial manipulator. Extended state observer was designed and implemented for contact torque estimation in [14-16]. A disturbance observer was proposed for interactive torques and friction forces estimation in [17-18] for upper limb rehabilitation robot. Estimation of external forces exerted by the robot during friction stir welding processes was presented in [19] to ensure better tracking performance. Deep neural networks were proposed in [20] for force/torque estimation of robot end-effectors. A model-based compensation technique was introduced for estimation of environmental force in [21-22]. A task-oriented based on dynamics model learning and a robust disturbance state observer was Proposed in [23] for estimation of contact force of robot manipulator. Recently, a sensor-less force estimation using disturbance observer and neural learning of friction was presented in [24] for industrial robots. In another recent work, a sensor-less interaction force and environment stiffness have been estimated using impedance control [25].

Based on the literature review presented above, the hybrid impedance and position control (HIPC) were based on parallel connections of the two force controllers using switch. However, the switching process between the controllers must be fast enough to avoid discontinuity of control signal which could lead to unstable behavior. In addition, the switching process is based on a desired frequency, which should be selected by the duty ratio or selection matrix, this means that the mechanical properties of the environment must be known in advance so as to adjust the duty ratio or selection matrix in other to switch to the appropriate controller at the time of contact. A series connection between the two force controllers without a switch was proposed in [26-27], however, a fixed high gain of the HIPC parameters were used which consumed high control torque. In this work, the hybrid adaptive impedance and position-based admittance control (HAIPC) used was similar to the proposed HAIPC in [27] but, implemented on end-point robot which is normally controlled via cartesian coordinate hybrid impedance control. The main contribution of this work is on the implementation of the HAIPC to control the endpoint interaction force via the control of the robot joint's angles. The endpoint coordinates are not known but are obtained via the forward kinematics of the robot using the joint angles. In HAIPC two controllers were connected in series without the switching technique to avoid instability at the time of switching. Similarly, the mechanical properties of the environment do not need to be known using the proposed HAIPC. Furthermore, the proposed method is cost effective since observer was used for contact torque/force estimation which eliminated the need for torque/force sensor, and it consumed less control torque which implies high energy saving and less cost for power consumptions.

It was also found in the literature that most of the contact force/torque estimation were conducted based on fixed mechanical properties of the environment. However, for upper-limb rehabilitation robot the damping and stiffness of the contact force/torque differs from one patient to another depending on the level of patient recovery stage and applied force. Therefore, the impedance control performance can be improved if the damping and stiffness are not kept constant. Thus, the focus of this research work was based on the estimation of environmental contact force/torque to update the damping and stiffness in the adaptive impedance controller. Therefore, the system would adapt based on the magnitude of the contact force/torque which varies from patient to patient. To the best of our findings on the existing literature this technique has not been use on upper-limb end-point robot for rehabilitation exercise. Hence, the contribution of this work is on the application of the new proposed HAIPC.

2.0 Mathematical Modelling

The mathematical model of the physical system of the upper-limb rehabilitation robot in our laboratory is obtained for the controller design. The robot's links, parameters, mass, and motor moments of inertia were measured experimentally to be used in the simulation.

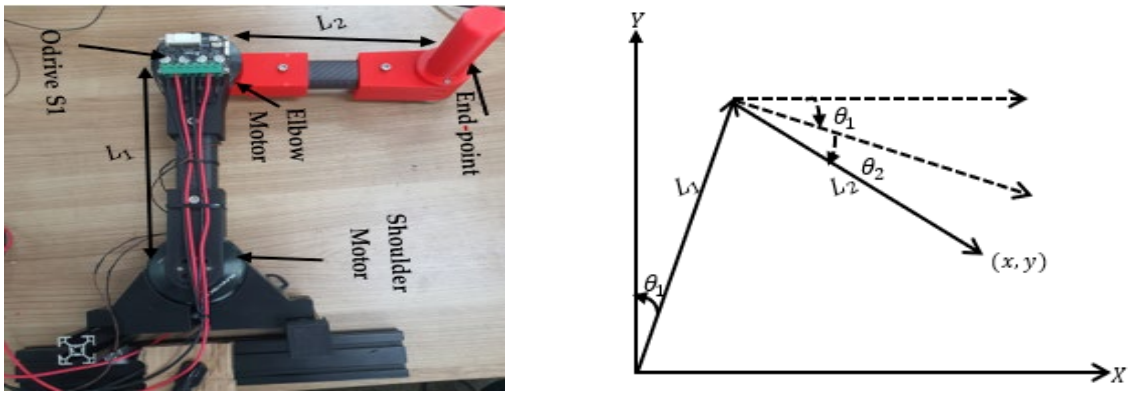

(a) (b)

Figure 1: Upper limb desktop rehabilitation robot (a) Physical system and (b) schematic diagram

Received: 26/03/2026; Revised: 20/04/2026; Accepted: 21/04/2026; Published: 25/04/2026

The Lagrange method was used to derive the mathematical model of the system in this work. Therefore, there is a need to compute the kinetic energy and potential energy of the system. The end-point upper limb rehabilitation robot considered in this work is shown in Figure 1 (a) and the schematic diagram in Figure 1 (b).

Using the Lagrangian function

$$\tau = \frac{d}{dt}\left(\frac{\partial T}{\partial \dot{q}}\right) - \frac{\partial T}{\partial q} \tag{1}$$

Total torque is given by

$$T = T_1 + T_2 + T_e \tag{2}$$

$$T_1 = \frac{1}{2} I_1 \dot{\theta}_1^2 + \frac{1}{2} m_2 (l_1 \dot{\theta}_1)^2 \tag{3}$$

$$T_2 = \frac{1}{2} I_2 \dot{\theta}_2^2 \tag{4}$$

$$T_e = \frac{1}{2} m_e V^2 = \frac{1}{2} m_e \dot{r}_e^2 \tag{5}$$

To obtain the kinetic energy of the system, the angular velocity of the joint link is required. Thus, the angular velocities in x and y directions are as follows;

$$r_e = [l_1 sin\theta_1 + l_2 \cos(\theta_1 + \theta_2)]\hat{\imath} + [l_1 cos\theta_1 - l_2 \sin(\theta_1 + \theta_2)]\hat{\jmath} \tag{6}$$

$$\dot{r}_e = \left[l_1 \dot{\theta}_1 cos\theta_1 - l_2 \sin(\theta_1 + \theta_2)\left(\dot{\theta}_1 + \dot{\theta}_2\right)\right]\hat{\imath} + \left[-l_1 \dot{\theta}_1 sin\theta_1 - l_2 \cos(\theta_1 + \theta_2)\left(\dot{\theta}_1 + \dot{\theta}_2\right)\right]\hat{\jmath} \tag{7}$$

$$\dot{r}_e{}^2 = \left[l_1 \dot{\theta}_1 cos\theta_1 - l_2 \sin(\theta_1 + \theta_2)\left(\dot{\theta}_1 + \dot{\theta}_2\right)\right]^2 + \left[-l_1 \dot{\theta}_1 sin\theta_1 - l_2 \cos(\theta_1 + \theta_2)\left(\dot{\theta}_1 + \dot{\theta}_2\right)\right]^2 \tag{8}$$

$$\dot{r}_e{}^2 = l_1^2 \dot{\theta}_1^2 + l_2^2 (\dot{\theta}_1 + \dot{\theta}_2)^2 - 2 l_1 l_2 \dot{\theta}_1 sin\theta_2 \tag{9}$$

$$T = \frac{1}{2} I_1 \dot{\theta}_1^2 + \frac{1}{2} m_2 (l_1 \dot{\theta}_1)^2 + \frac{1}{2} I_2 \dot{\theta}_2^2 + \frac{1}{2} m_e (l_1^2 \dot{\theta}_1^2 + l_2^2 (\dot{\theta}_1 + \dot{\theta}_2)^2 - 2 l_1 l_2 \dot{\theta}_1 \left(\dot{\theta}_1 + \dot{\theta}_2\right) sin\theta_2) \tag{10}$$

Since, the robot is planer root the potential energy is assumed to be zero

$$P = 0 \tag{11}$$

Using equation (1) above, the equation of motion for link 1 and link 2 are as follows.

$$(\tau_1 - \tau_2) = \frac{d}{dt}\left(\frac{\partial T}{\partial \dot{\theta}_1}\right) - \frac{\partial T}{\partial \theta_1} \tag{12}$$

$$(\tau_1 - \tau_2) = (I_1 + m_2 {l_1}^2 + m_e (l_1^2 + l_2^2) - 2 m_e l_1 l_2 sin\theta_2)\ddot{\theta}_1 + (m_e l_2^2 - m_e l_1 l_2 sin\theta_2)\ddot{\theta}_2 - 2 m_e l_1 l_2 \dot{\theta}_1 \dot{\theta}_2 cos\theta_2 - m_e l_1 l_2 \dot{\theta}_2{}^2 cos\theta_2 \tag{13}$$

$$\tau_2 = \frac{d}{dt}\left(\frac{\partial T}{\partial \dot{\theta}_2}\right) - \frac{\partial T}{\partial \theta_2} \tag{14}$$

$$\tau_2 = (m_e l_2^2 - m_e l_1 l_2 sin\theta_2)\ddot{\theta}_1 + (m_e l_2^2 + I_2)\ddot{\theta}_2 - 2 m_e l_1 l_2 \dot{\theta}_1{}^2 cos\theta_2 \tag{15}$$

Generally, the system equation can be represented as follows:

$$M(\theta)\ddot{\theta} + C\left(\theta, \dot{\theta}\right)\dot{\theta} + G(\theta) = \tau \tag{16}$$

where $M(\theta)$, $C\left(\theta, \dot{\theta}\right)$, $G(\theta)$ and τ are the mass/moment of inertia of the links and motors matrix, *C* is centrifugal and Coriolis force, *G* contains the gravitational term and the total control torque.

3.0 Control Design

The proposed control is a hybrid adaptive impedance and position control (HAIPC). The adaptive impedance control was designed to regulate the contact torques applied by the patients during interaction with the

Received: 26/03/2026; Revised: 20/04/2026; Accepted: 21/04/2026; Published: 25/04/2026

rehabilitation robot. It is expected that different patients would have different contact torques depending on their intended motion and level of recovery. The changes in contact torque were used to update the damping and stiffness at the robot joints in order to produce efficient human-robot interaction and compliance. On the other hand, Admittance control with the GA_PD controller was designed for desired trajectory position tracking. The proposed control is an improved work in [26]. Figure 2 shows the block diagram of the HIPC proposed in [26], and Figure 3 shows the improved HAIPC controller used in this work.

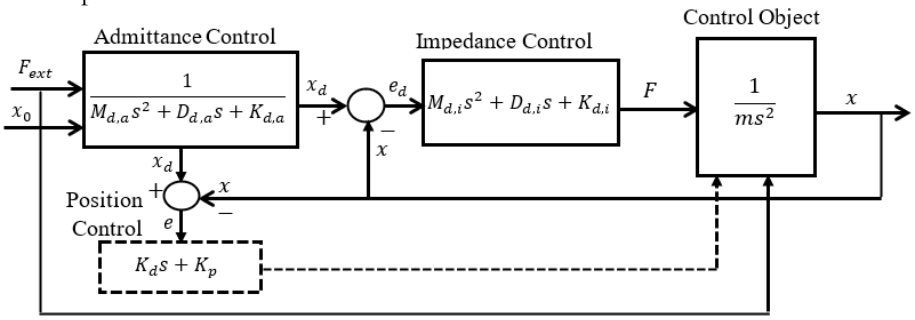

Figure 2: Hybrid impedance and position control HIPC by [26]

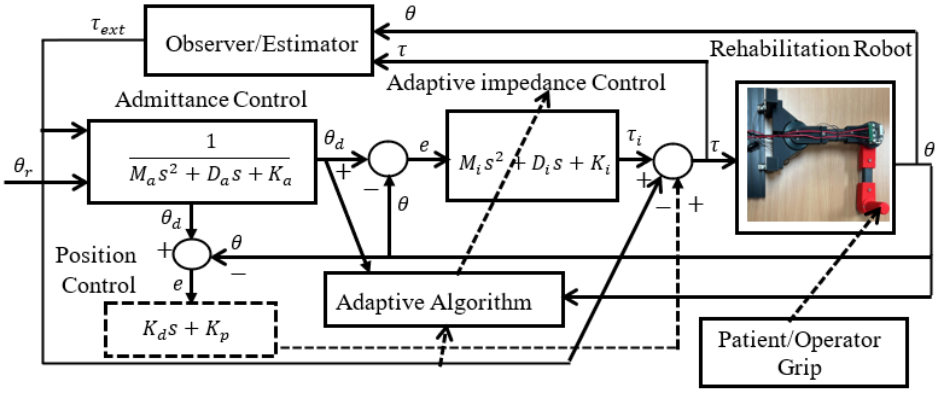

Figure 3: Hybrid adaptive impedance and position control (HAIPC)

3.1 Control Design

This work used a PD controller in series with admittance control for desired position tracking control of the two links' joint angles. Genetic Algorithm (GA) optimization was used to obtain the optimal values of the PD gains for proper trajectory tracking. The admittance control based on the estimated contact torque generates a desired reference position, which PD control tracks to guide the patient's hand along the desired trajectory. Therefore, the position controller is the GA_PD controller.

$$PD = K_p e(t) + +K_d \frac{d}{dt} e(t) \tag{17}$$

The PID controller parameters were optimized using a Genetic Algorithm (GA) based on a performance-driven fitness function. Specifically, the objective function was formulated to minimize the Integrated Absolute Error (IAE) of the tracking response for both x- and y-axes. The fitness function is defined as the cumulative sum of the absolute difference between the reference and actual system outputs over the simulation horizon, expressed as

$$J = \sum_{t=0}^{T} \left(\mid e_x(t) \mid + \mid e_y(t) \mid \right) \tag{18}$$

where $e_x(t)$and $e_y(t)$denote the tracking errors in the x- and y-directions, respectively. The GA searches for the optimal set of PID gains $\left[K_{p_x}, K_{i_x}, K_{d_x}, K_{p_y}, K_{i_y}, K_{d_y}\right]$within predefined bounds. In this study, the search ranges were selected as $K_p \in [K_p^{\min}, K_p^{\max}]$, $K_i \in [K_i^{\min}, K_i^{\max}]$, and $K_d \in [K_d^{\min}, K_d^{\max}]$, chosen based on system stability considerations and prior tuning experience. This formulation ensures that the optimisation process systematically improves tracking accuracy while maintaining feasible and stable controller parameters.

In the hardware, motor 1 has a higher rating and weight compared to motor 2, which is smaller in size with less torque. This is because motor 2 is situated at the end of link 1 (elbow joint), and if a heavy motor is used, it

Received: 26/03/2026; Revised: 20/04/2026; Accepted: 21/04/2026; Published: 25/04/2026

may cause too much vibration, and high torque will be needed to move motor 1 at the first joint. The admittance control equation is represented as follows;

$$M_a\ddot{\theta}_d + D_a\dot{\theta}_d + K_a(\theta_d - \theta_r) = \tau_{ext} \tag{19}$$

3.2 Contact Torque Estimation

The system has no contact torque/force sensor to measure the interaction torque/force at the robot joints. Therefore, an extended state observer was used to estimate the contact torque. The equation of joint contact torque is given by:

$$K(\theta_d - \theta_e) = \tau_{ext} \tag{20}$$

Let the robot model be considered as a second-order system:

$$\ddot{\theta}(t) = \tau_{ext} + bu(t) \tag{21}$$

The state space joint angle equations are as follows:

$$\dot{\theta}_1(t) = \theta_2(t) \tag{22}$$

$$\dot{\theta}_2(t) = \rho u(\theta, t) + \tau_{ext} \tag{23}$$

State space equations can be extended to include environmental contact torque as a new state, variable that acts as an external torque acting on the robot $\vartheta_3 = \tau_{ext}$ which yields the following:

$$\dot{\vartheta}_3(t) = \dot{\tau}_{ext}(\theta, t) \tag{24}$$

Thus, the extended state observer can be designed as follows:

$$\dot{\hat{\theta}}_1(t) = \hat{\theta}_2(t) + b_1\hat{e}(t) \tag{25}$$

$$\dot{\hat{\theta}}_2(t) = \hat{\vartheta}_3(t) + b_2\hat{e}(t) + \rho u(\theta, t) \tag{26}$$

$$\dot{\hat{\vartheta}}_3(t) = b_3\hat{e}(t) \tag{27}$$

Where the estimate and actual systems states are $\hat{\theta}_1(t), \hat{\theta}_2(t), \hat{\vartheta}_3(t)$ and $\theta_1(t), \theta_2(t), \vartheta_3(t)$, respectively. The observer gains are b_1, b_2, b_3, and the observer error is given by $\hat{e}(t) = \hat{\theta}_1(t) - \theta_1(t)$. The observer gains were designed separately for link 1 and link 2 based on the general assumption that the observer poles should be placed four to ten times to the left of the s-plane of the closed loop poles for faster response (i.e $\omega_{obs} = (4 - 10)\omega_c$). Thus, in this work $\omega_{obs} = 6 * \omega_c$ was chosen to get the gains as follows:
$b_{m11} = 3\omega_{obs},\ b_{m12} = 3{\omega_{obs}}^2,\ b_{m13} = 3{\omega_{obs}}^3$ and $b_{m21} = 3\omega_{obs},\ b_{m22} = 3{\omega_{obs}}^2,\ b_{m23} = 3{\omega_{obs}}^3$
Therefore, the observer gain matrix is given by the following:

$$L = \begin{bmatrix} b_{m11} & b_{m12} & b_{m13} & 0 & 0 & 0 \\ 0 & 0 & 0 & b_{m21} & b_{m22} & b_{m23} \end{bmatrix}^T \tag{28}$$

3.3 Adaptive Impedance Control

The dynamic model of the robot in Equations (13) and (15) with total control torque and estimated contact torque can be expressed as:

$$M(\theta)\ddot{\theta} + C\left(\theta, \dot{\theta}\right)\dot{\theta} + G(\theta) = \tau - \tau_{ext} \tag{29}$$

Where *M is* the mass and moment of inertia matrix, *C* represents centrifugal and Coriolis force, and *G* is the gravitational force. The terms τ and τ_{ext} are the system input torque and estimated environmental contact torque, respectively. The contact torque was estimated in section 3.2; this estimated torque is used as input to the admittance control and the adaptive algorithm to update the damping and stiffness gains. Recursive least-square algorithm was used for tuning of the damping and stiffness constant (D and K) of the impedance controller based on changes in the environmental contact torque τ_d . The adaptive algorithm was formulated to update the parameters of the impedance control online based on changes in the contact torque for different patients. The impedance control is represented in Equation (30) as follows:

Received: 26/03/2026; Revised: 20/04/2026; Accepted: 21/04/2026; Published: 25/04/2026

$$M_i\left(\ddot{\theta}_d - \ddot{\theta}\right) + D_i\left(\dot{\theta}_d - \dot{\theta}\right) + K_i(\theta_d - \theta) = \tau_i \tag{30}$$

Where M_i, D_i and K_i are the inertia, damping, and stiffness coefficients of the impedance controller, and in this work, the inertia M_i was selected to be 1, and the damping and stiffness will be updated based on the adaptive algorithm using the estimated contact torque. Therefore, for the adaptive formulation, the impedance control was reduced as Equation (31) since $M_i = 1$.

$$D_i\left(\dot{\theta}_d - \dot{\theta}\right) + K_i(\theta_d - \theta) = \tau_{ext} \tag{31}$$

The human-robot interaction is assumed to be stiff therefore; the environmental contact torque is given by:

$$\tau_{ext} = K_e(\theta_d - \theta_e) \tag{32}$$

However, in this work, the environment is unknown, and therefore the τ_{ext} was estimated using the extended state observer and it will be used in the adaptive algorithm to update the damping and stiffness. The adaptive impedance controller law is as follows:

$$\widehat{D}\dot{e} + \widehat{K}e = \varphi^T(t)\hat{\sigma}(t) \tag{33}$$

where $\hat{\sigma}(t) = [\widehat{D} \quad \widehat{K}]$ represent estimation vector, $\varphi^T(t) = [e \quad \dot{e}]^T$ represent the regression vector, $\dot{e} = \left(\dot{\theta}_d - \dot{\theta}\right)$ and $e = (\theta_d - \theta)$.

$$\hat{\sigma}(t) = \hat{\sigma}(t-1) + J(t)[\tau_{ext} - \varphi^T(t)\hat{\sigma}(t-1)] \tag{34}$$

$$J(t) = \beta(t-1)\varphi(t)[1 + \varphi^T(t)\beta(t-1)\varphi(t)]^{-1} \tag{35}$$

$$\beta(t) = [I_2 - J(t)\varphi^T(t))]\beta(t-1) \tag{36}$$

$\beta(t)$ is a covariance 2 x 2 matrix with initial value $\beta(0) = \beta_0 I_2$, where β_0 is a positive large number, in this work $\beta_0 = 10^4$.

4.0 Result and Discussion

This section presents the simulation-based evaluation of the proposed HAIPC in comparison with the HIPC method in [26]. The contact torque illustrated in Fig. 4 represents the human–robot interaction force, which is unknown in real-time operation and is therefore estimated using an extended state observer (ESO) based on joint angular measurements. For simulation purposes, a known contact torque profile is applied. To reflect variations in patient capability, two representative torque levels (*3 Nm* and *5 Nm*) are considered. The interaction is evaluated under two modes: passive mode, where the patient is fully assisted by the robot during elliptical trajectory tracking of the shoulder and elbow joints, and active mode, where the patient actively applies torque to assist the motion.

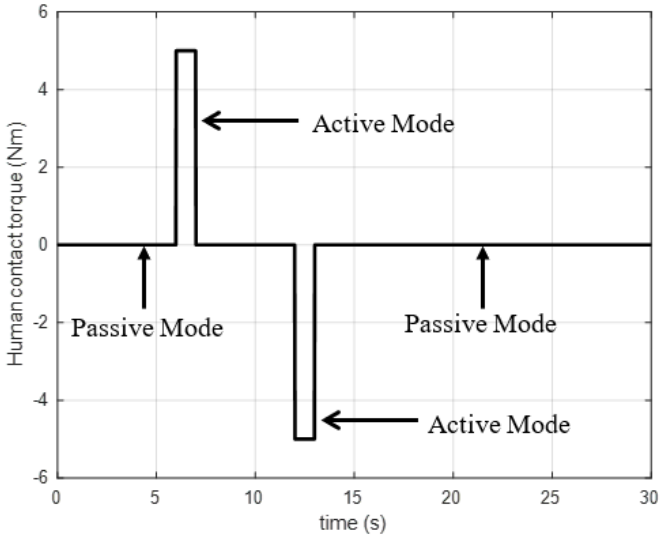

Figure 4: Human contact torque

4.1 Result Simulation

The GA_PD gains for motor 1 and motor 2 used in the simulation were obtained as $K_p = 50.2311$, $K_d = 8.5613$ and $K_p = 30.2311, K_d = 6.9613$ respectively. The simulation results were carried out with two different patients. First, the results were for the patient with *5 Nm* applied contact torque/force in active mode, and secondly, similar results were obtained with another patient who applied contact torque/force of *3 Nm*. In both cases, the joint's angular position trajectory tracking is shown while the contact force tracking was based on the ESO using the angular positions. The admittance control gains used were $M_a = 1, D_a = 2\sqrt{M_a K_a}$ and $K_a = 10$ for both HAIPC and HIPC controllers. Also, the impedance control gains for HIPC were $M_i = 1$, $D_i = 2 \times 0.7 \times \sqrt{M_i K_i}$ and $K_i = 100$. The HAIPC impedance control gains were updated online during the human-robot interaction which would be discussed later.

4.1.1 Case I: With Patient Contact Torque of *5 Nm*

The patient applied contact torque in case I as shown in Figure 4. Human-robot interaction is of two modes; the passive mode in which the patient therapy is completely assisted by the robot. In this mode, the patient only holds and follows the robot's end-point motion along the ellipse path. The patient's shoulder and elbow joints undergo physical therapy to recover the joints' functioning abilities. On the other hand, in active mode, the patient applied some force to strengthen his arm during the therapy and observe his level joint functionality recovery. Figures 5 (a) and (b) show the desired angular position tracking for joint 1 and 2 respectively. The black line represents the reference angular position input θ_r to the system which the admittance control used to generate the desired angular position θ_d to be tracked by θ using the HAIPC and HIPC controls. It can be observed that from *0 s* to *6 s* and *13 s* to *30 s* the patient was in passive mode. During this time the patient applied zero torque and therefore, the robot moved the patient's arm with the help of the robot end-point griper to follow the ellipse path as shown in Figures 6 (a) and (b).

Similarly, from *6 s* to *7 s* and from *12 s* to *13 s* the patient is in active mode with applied contact torque of *5 Nm* hence, the desired angular position θ_d generates by the admittance changed to a new position based on the contact torque applied. Thus, the proposed method HAIPC and HIPC produced a measured angular position θ in compliance to the applied contact torque to track θ_d. It was found that in both angular position tracking in Figures 5 (a) and (b) and end-point position tracking in Figures 6 (a) and (b) the two controllers HAIPC and HIPC tracked the desired trajectory with position tracking sum of absolute error (SAE) of *0.300 m* and *0.241 m* respectively. This shows that the HIPC performed better with minimum SAE in position tracking as compared to proposed HAIPC. However, in upper-limb rehabilitation exercise this difference is not significant in fact in real-time it's difficult to notice the difference. The superiority of the proposed HAIPC as compared to HIPC is as shown in Figure 7 (a) and (b) in terms of energy consumption. It was found that the HIPC consumed high control torque especially at beginning of the exercise. The SAE of the control signals of HAIPC and HIPC were measured as *8.563 Nm* and *14.025 Nm* respectively. This result yields *63.79%* reduction in the control torque consumption using the proposed method HAIPC as compared to HIPC. This advantage would significantly improve the life span of the system and its cost effective for both hospitals and private homes therapy. In addition, the HAIPC eliminate the needs for contact torque/force sensor thereby reducing the cost of the robot construction.

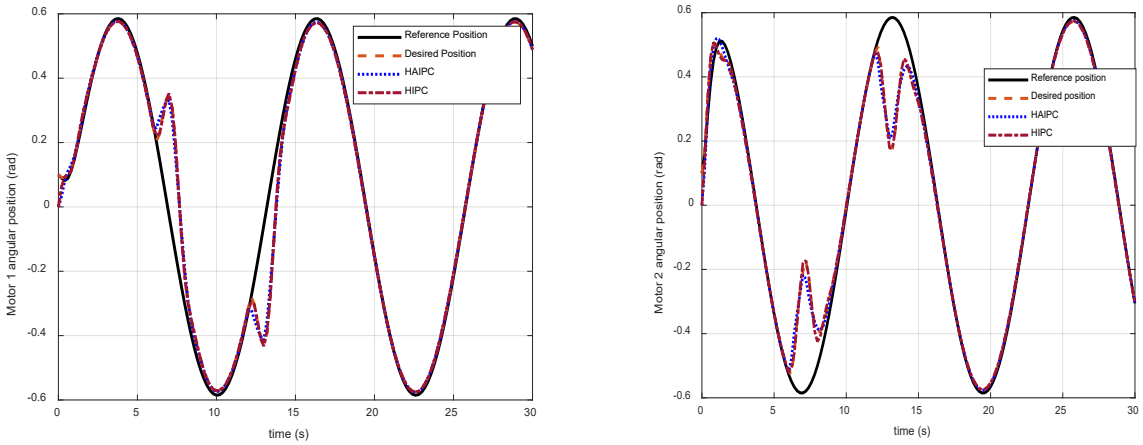

(a) (b)

Figure 5: Angular Position (a) for motor 1 and (b) for motor 2

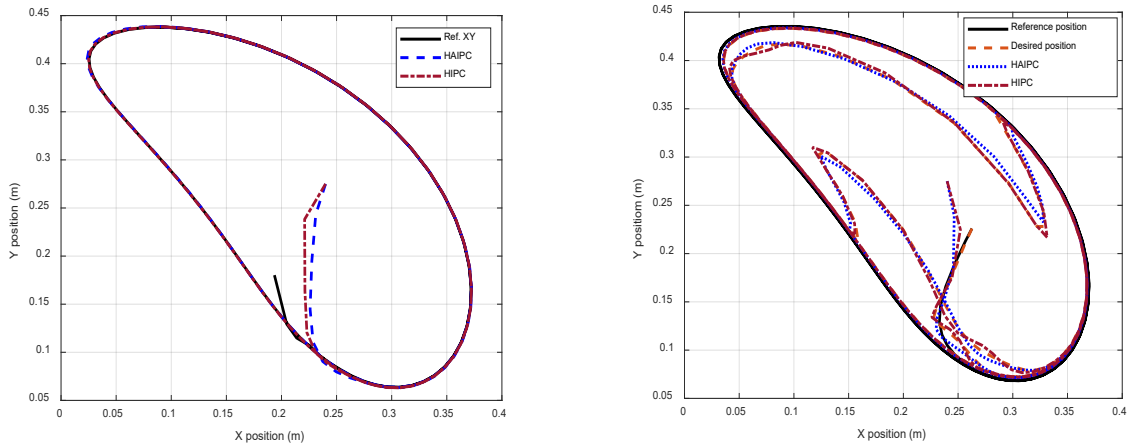

(a) (b)

Figure 6: End-Point Position XY (a) No Contact Torque and (b) with 5 Nm Contact Torque

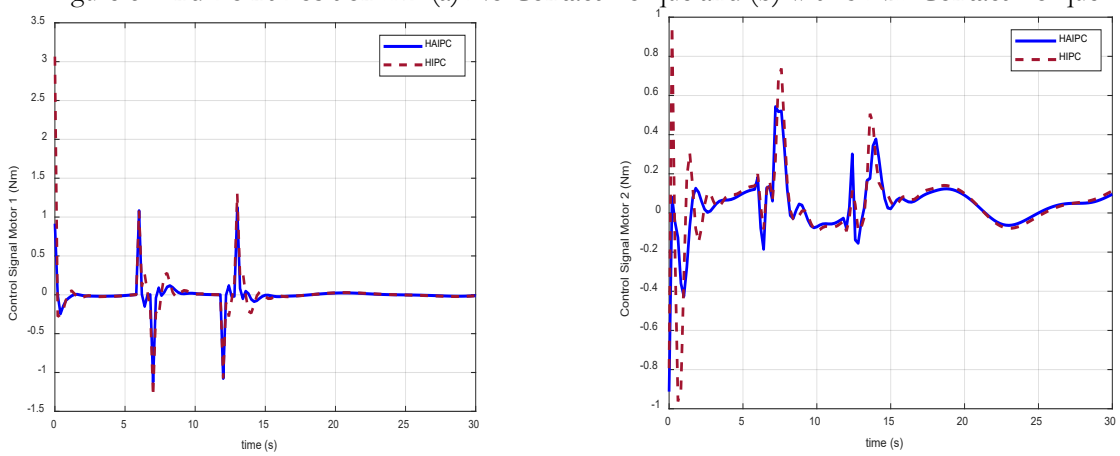

(a) (b)

Figure 7: Control Signal (a) for motor 1 and (b) for motor 2

As mentioned earlier, in upper-limb rehabilitation robot the magnitude of the human-robot interaction torque is unknown in real-time and therefore, ESO was used to estimate it along the angular position. To demonstrate the effectiveness of the ESO estimation a known desired contact torque was used in the simulation. Figure 8 (a) and (b) shows the estimated torque tracking the desired known torque. It was observed that the HAIPC provides better torque tracking as compared to HIPC. The tracking error is shown in Figure 9 (a) and (b) with the SAE of *82.16* and *95.55* for HAIPC and HIPC respectively.

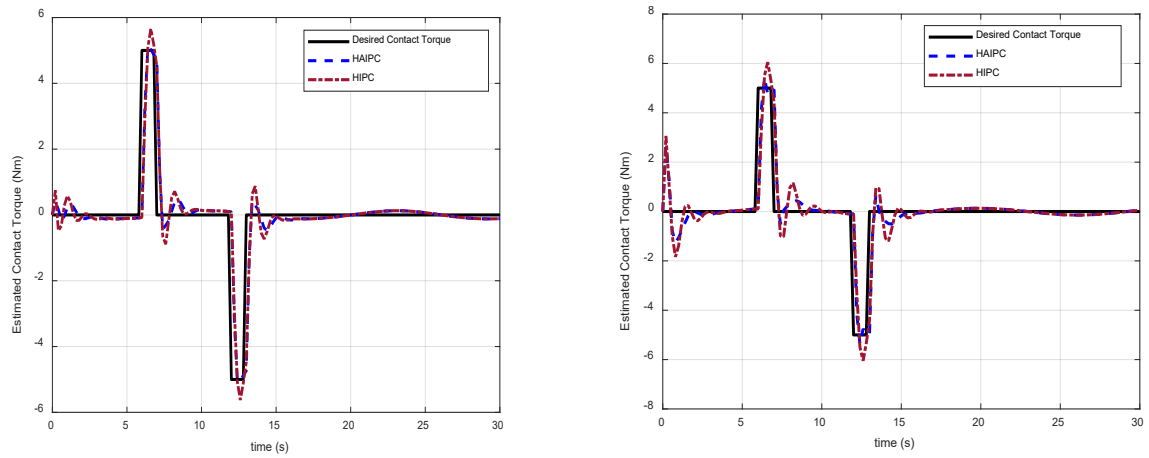

(a) (b)

Figure 8: Estimated Contact Torque (a) for motor 1 and (b) for motor 2

Received: 26/03/2026; Revised: 20/04/2026; Accepted: 21/04/2026; Published: 25/04/2026

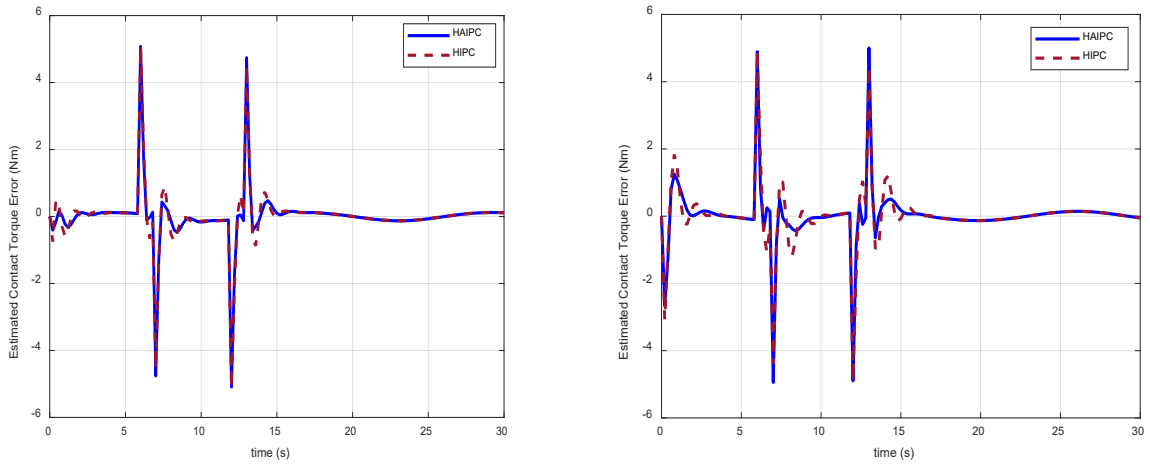

(a) (b)

Figure 9: Estimated Contact Torque Error (a) for motor 1 and (b) for motor 2

The adaptive parameters are shown in Figure 10 (a) and (b) for joints 1 and 2. The desired human torque was in active mode from *6 s* to *7 s* and from *12 s* to *13 s*. It was observed that the damping and stiffness changed to provides the complaint. From *6 s* to *7 s* in Figure 10 (a) and (b) it was found that the damping of joints 1 and 2 changed to *-0.871 Ns/m* and *-0.584 Ns/m* and the stiffness of joints 1 and 2 changed to *-6.872 N/m* and *8.953 N/m* respectively. Similarly, from *12 s* to *13 s* the damping and stiffness changes to *0.391 Ns/m, 1.00 Ns/m* and *-7.021 N/m, 12.893 N/m* respectively. Figures 11 (a) and (b) shows the impedance control torque for the two controls. It was observed that the HIPC has the peak torque as compared to HAIPC.

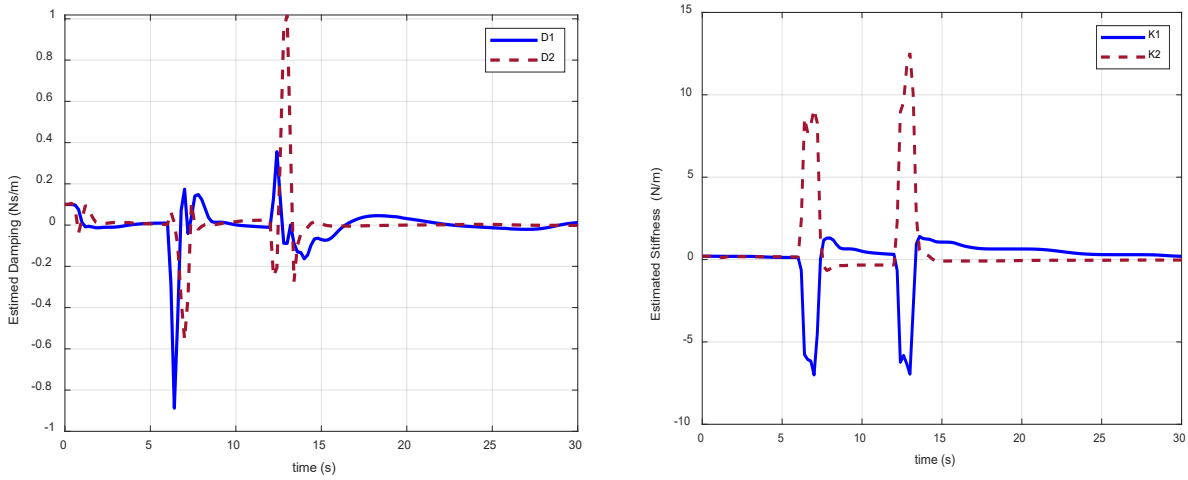

(a) (b)

Figure 10: Adaptive Parameters (a) Estimated Damping and (b) Estimated Stiffness

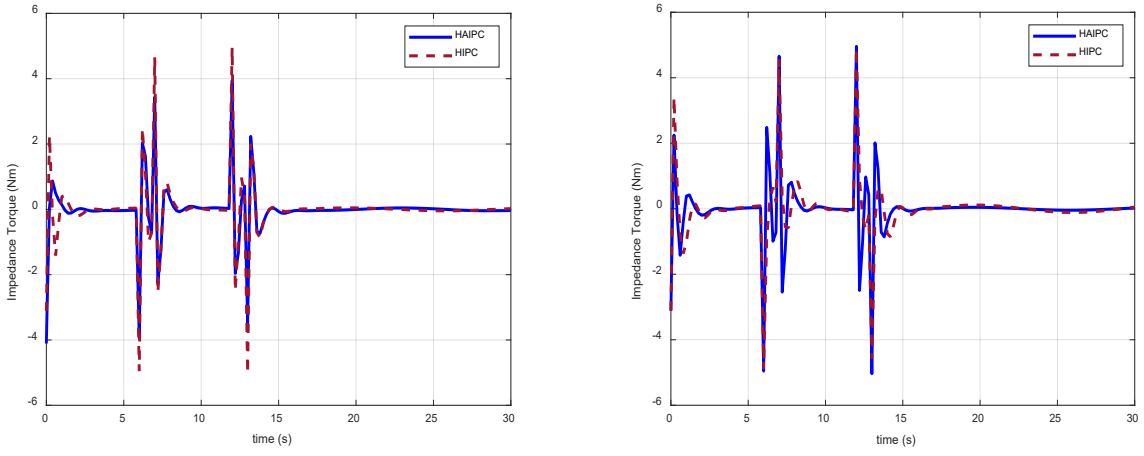

(a) (b)

Figure 11: Impedance Torque (a) Motor 1 and (b) Motor 2

4.1.2 Case II: Patient with Contact Torque of *3 Nm*

Results consistent with Case I were observed. The SAE of the control signals for both HAIPC and HIPC, obtained from Figs. 12(a) and 12(b), are summarized in Table II. The angular and endpoint tracking performances are illustrated in Figs. 13(a)–(b) and Figs. 14(a)–(b), respectively, with the corresponding tracking errors also reported in Table II. Torque estimation performance is shown in Figs. 15(a) and 15(b), where HAIPC demonstrates superior tracking of the desired torque compared to HIPC. The tracking error profiles in Figs. 16(a) and 16(b) yield SAE values of *58.702* and *63.480* for HAIPC and HIPC, respectively. The evolution of adaptive parameters for joints 1 and 2 is presented in Figs. 17(a) and 17(b). During active interaction intervals (*6–7 s* and *12–13 s*), variations in stiffness and damping parameters enable compliant behavior. Furthermore, Figs. 18(a) and 18(b) show the impedance control torque, where HIPC exhibits higher peak torque, particularly at the second joint, compared to HAIPC.

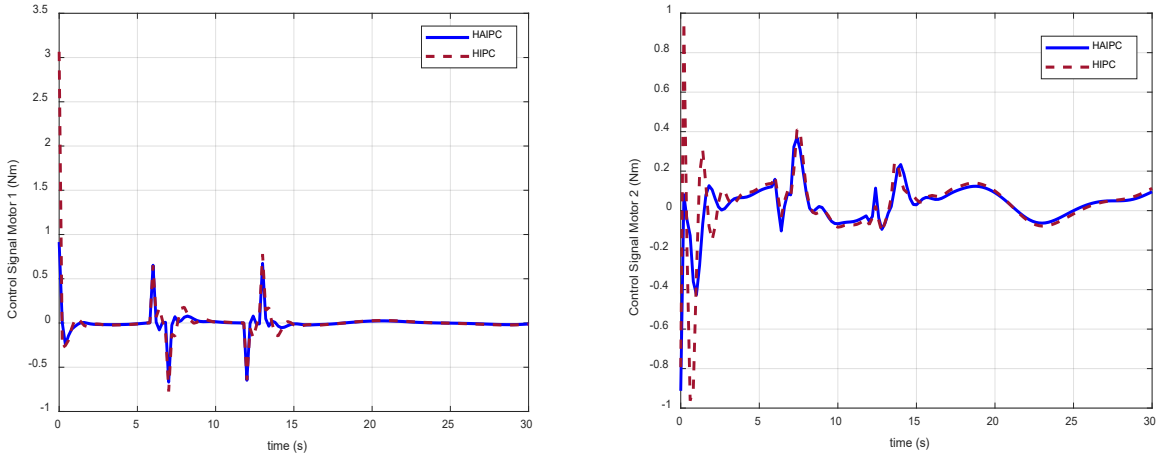

(a) (b)

Figure 12: Control Signal (a) for motor 1 and (b) for motor 2

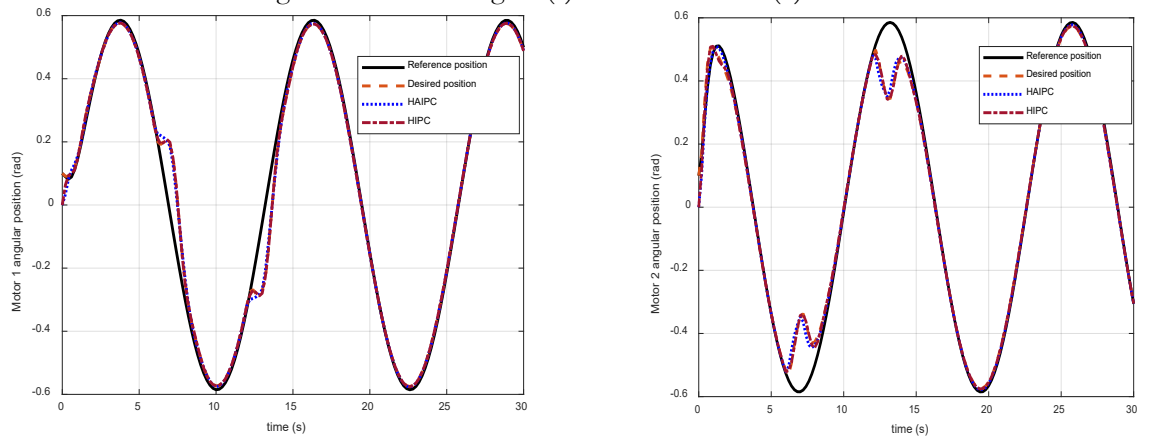

(a) (b)

Figure 13: Angular Position (a) for motor 1 and (b) for motor 2

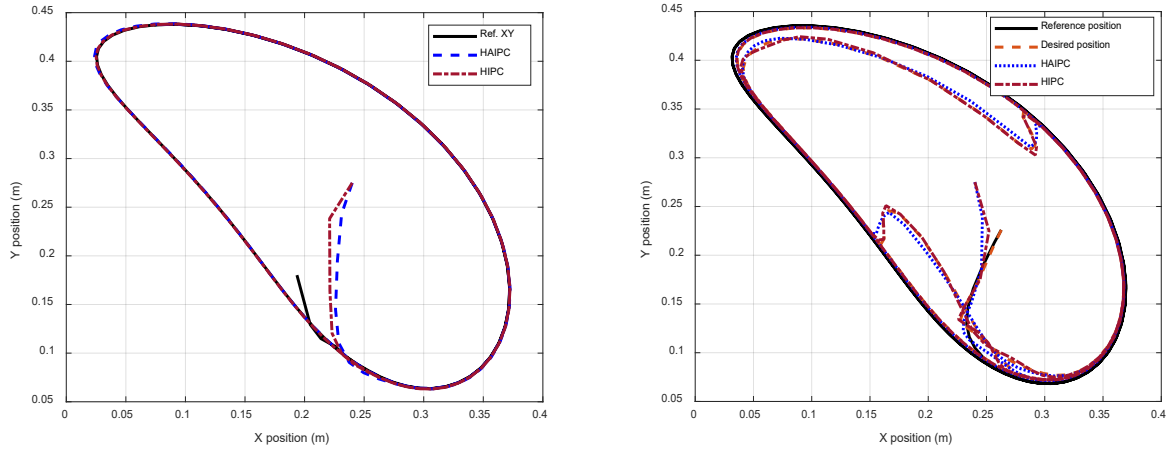

(a) (b)

Figure 14: End-Point Position XY (a) No Contact Torque and (b) 3 Nm Contact Torque

Received: 26/03/2026; Revised: 20/04/2026; Accepted: 21/04/2026; Published: 25/04/2026

Table 2: Results with Contact Torque of 3 Nm

Control Methods	Control Signal SAE	Contact Torque Error SAE	End-Point Tracking Error SAE
HAIPC	6.274	58.702	0.206
HIPC	10.633	63.480	0.150

*Square Absolute Error (SAE)

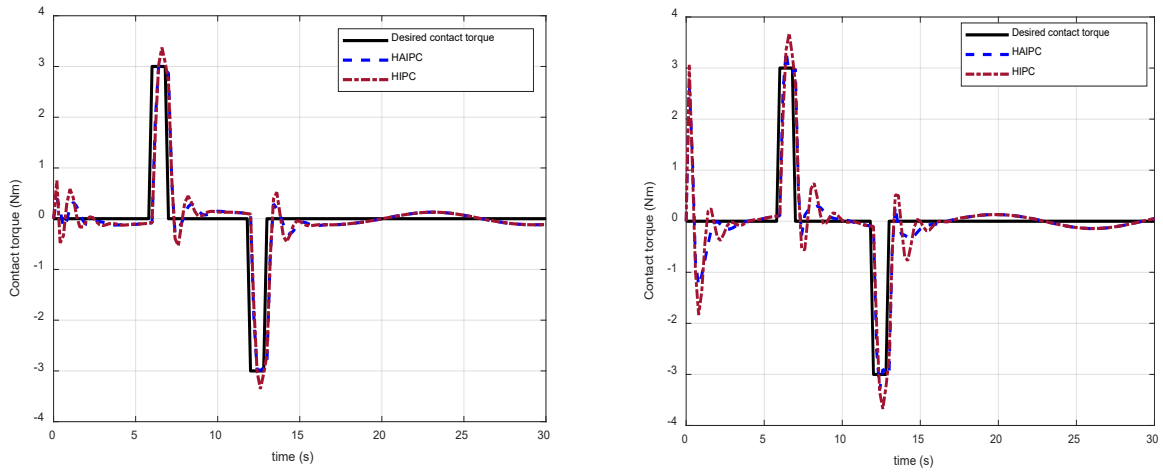

(a) (b)

Figure 15: Estimated Contact Torque (a) for motor 1 and (b) for motor 2

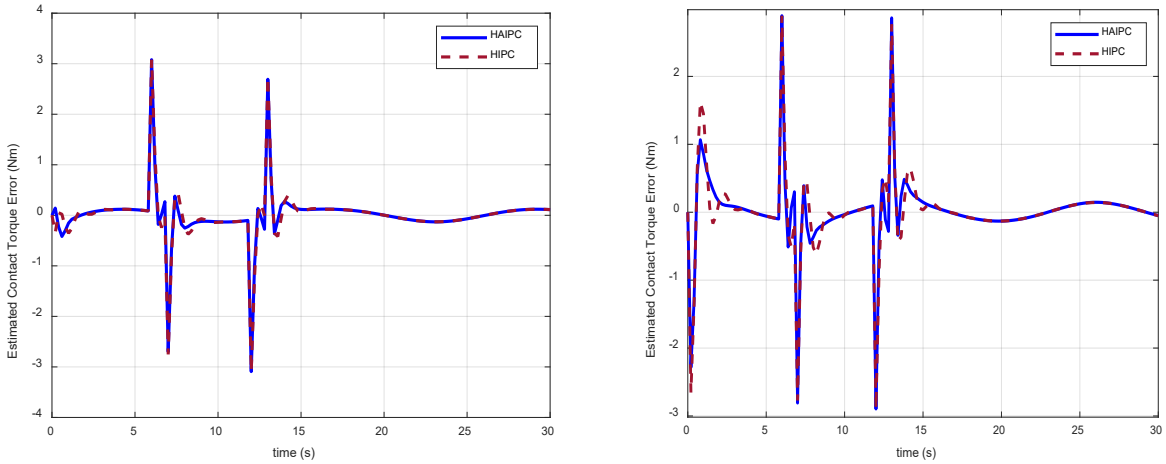

(a) (b)

Figure 16: Estimated Contact Torque Error (a) for motor 1 and (b) for motor 2

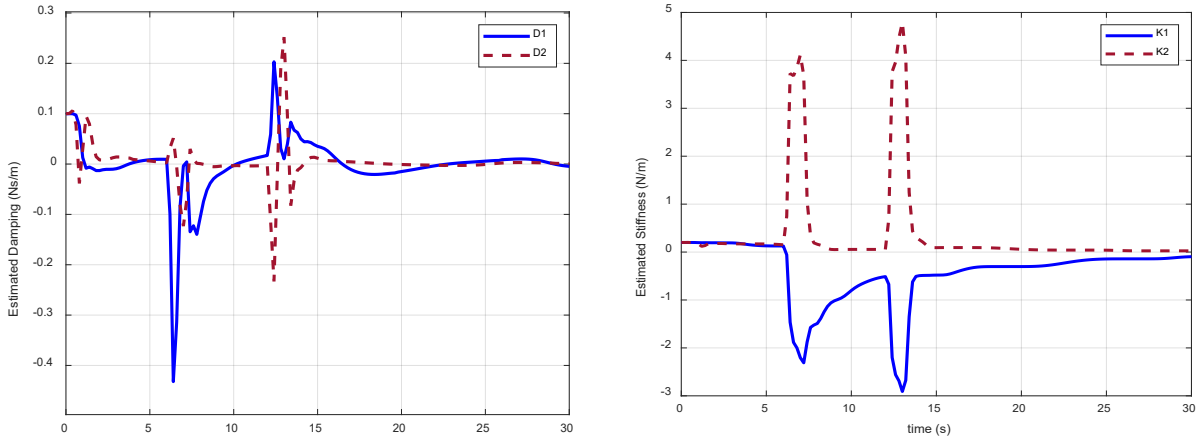

(a) (b)

Figure 17: Adaptive Parameters (a) Estimated Damping and (b) Estimated Stiffness

Received: 26/03/2026; Revised: 20/04/2026; Accepted: 21/04/2026; Published: 25/04/2026

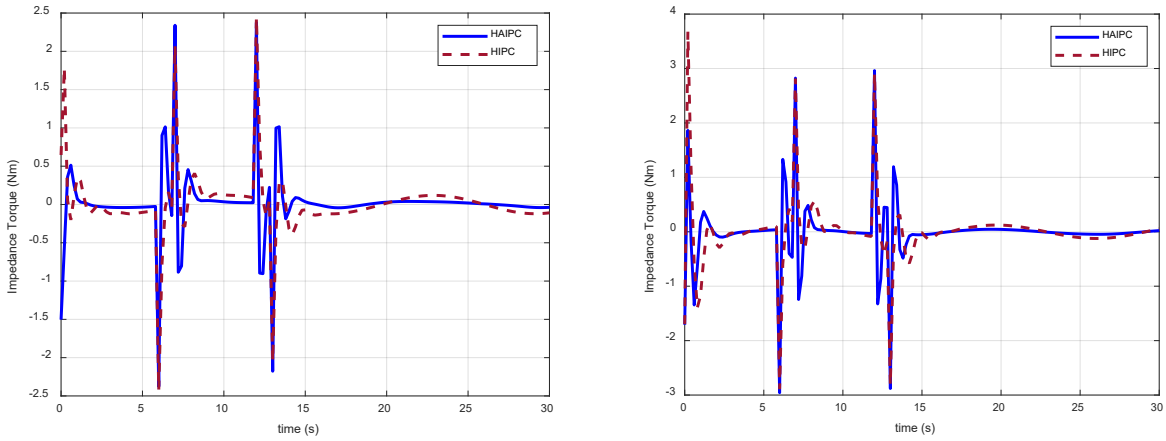

(a) (b)

Figure 18: Impedance Torque (a) Motor 1 and (b) Motor 2

5.0 Conclusion

The proposed series Hybrid Adaptive Impedance Control (HAIPC) demonstrates a robust and effective solution for compliant control of end-point rehabilitation robots via joint-level implementation. Comparative results clearly establish that HAIPC significantly enhances torque tracking performance, reduces torque estimation error, and improves energy efficiency relative to conventional Hybrid Impedance Control (HIPC), as quantified by the Sum of Absolute Error (SAE). This improvement is consistently observed across both passive and active rehabilitation modes, including interaction scenarios with contact torques of *3 Nm* and *5 Nm*. Notably, a minor trade-off is identified in position tracking accuracy, where HIPC exhibits marginally better performance. The series control architecture, implemented without any switching mechanism, effectively eliminates the instability and discontinuity issues commonly associated with parallel hybrid controllers, ensuring smooth and stable system behavior. These results highlight the strong potential of HAIPC for safe and adaptive human-robot interaction. Future work will focus on real-time experimental validation and large-scale clinical assessment.

References

[1] N. Hogan, "Impedance control: An approach to manipulation," in *1984 Am. Control Conf.*, San Diego, CA, USA, 1984, pp. 304–313, doi: 10.23919/ACC.1984.4788393.

[2] N. Hogan, "The mechanics of multi-joint posture and movement control," *Biol. Cybern.*, vol. 52, no. 5, pp. 315–331, 1985, doi: 10.1007/BF00355754.

[3] A. Rabaseda, E. Seguin, and M. Doumit, "Enhancing human mobility exoskeleton comfort using admittance controller," *WSEAS Trans. Biol. Biomed.*, vol. 18, pp. 24–31, 2021.

[4] C. Ott, R. Mukherjee, and Y. Nakamura, "A hybrid system framework for unified impedance and admittance control," *J. Intell. Robot. Syst.*, vol. 78, pp. 359–375, 2015, doi: 10.1007/s10846-014-0082-1.

[5] R. Anderson and M. W. Spong, "Hybrid impedance control of robotic manipulators," *IEEE J. Robot. Autom.*, vol. 4, no. 5, pp. 549–556, 1988.

[6] G. J. Liu and A. A. Goldenberg, "Robust hybrid impedance control of robot manipulators," in *Proc. IEEE Int. Conf. Robot. Autom.*, California, USA, 1991, pp. 287–292.

[7] E. Akdoğan, M. A. Arslan, O. Kuran, and M. E. Tatlıcıoğlu, "Hybrid impedance control of a robot manipulator for wrist and forearm rehabilitation: Performance analysis and clinical results," *Mechatronics*, vol. 49, pp. 77–91, Jul. 2018.

[8] Y. Kim, "Hybrid-mode impedance control for position/force tracking in motor-system rehabilitation," *Int. J. Adv. Robotic Syst.*, vol. 12, no. 6, 2015, doi: 10.5772/60968.

[9] Y. Oh, W. K. Chung, Y. Youm, and I. H. Suh, "Motion/force decomposition of redundant manipulators and its application to hybrid impedance control," in *Proc. IEEE Int. Conf. Robot. Autom.*, Leuven, Belgium, 1998, pp. 1441–1446.

[10] J. Wang and Y. Li, "Hybrid impedance control of a 3-DOF robotic arm used for rehabilitation treatment," in *Proc. 2010 IEEE Int. Conf. Autom. Sci. Eng.*, Toronto, ON, Canada, 2010, pp. 768–773, doi: 10.1109/COASE.2010.5584259.

[11] O. S. Ajani and S. F. M. Assal, "Hybrid force tracking impedance control-based autonomous robotic system for tooth brushing assistance of disabled people," *IEEE Trans. Med. Robot. Bionics*, vol. 2, no. 4, pp. 649–660, Nov. 2020, doi: 10.1109/TMRB.2020.3030317.

[12] G. Bätz, B. Weber, M. Scheint, D. Wollherr, and M. Buss, "Dynamic contact force/torque observer: Sensor fusion for improved interaction control," *Int. J. Robot. Res.*, 2013, doi: 10.1177/0278364913482015.

Received: 26/03/2026; Revised: 20/04/2026; Accepted: 21/04/2026; Published: 25/04/2026

[13] C. Feng, D. Paul, N. Siliang, and C. XiaoQi, "Contact force and torque sensing for serial manipulator based on an adaptive Kalman filter with variable time period," *Robot. Comput.-Integr. Manuf.*, vol. 73, 2021, doi: 10.1016/j.rcim.2021.102210.

[14] C. Chao, Z. Chengrui, H. Tianliang, N. Hepeng, and L. WeiChao, "Model-assisted extended state observer-based computed torque control for trajectory tracking of uncertain robotic manipulator systems," *Int. J. Adv. Robotic Syst.*, vol. 15, no. 5, 2018, doi: 10.1177/1729881418801738.

[15] S. Gijo, L. Zeyu, C. Vincent, K. Demy, T. Ying, and O. Denny, "Interaction force estimation using extended state observers: An application to impedance-based assistive and rehabilitation robotics," *IEEE Robot. Autom. Lett.*, vol. 4, no. 2, pp. 1156–1161, 2019.

[16] A. M. Abdullahi and R. Chaichaowarat, "Sensorless estimation of human joint torque for robust tracking control of lower-limb exoskeleton assistive gait rehabilitation," *J. Sens. Actuator Netw.*, vol. 12, no. 4, pp. 1–27, 2023, Art. no. 53.

[17] L. Xiangxing, Z. Guokun, Z. Jiaji, and W. Jiajin, "Sensorless force estimation of end-effect upper limb rehabilitation robot system with friction compensation," *Int. J. Adv. Robotic Syst.*, vol. 16, no. 3, 2019, doi: 10.1177/1729881419856132.

[18] W. Liang, S. Huang, S. Chen, and K. K. Tan, "Force estimation and failure detection based on disturbance observer for an ear surgical device," *ISA Trans.*, vol. 66, pp. 476–484, 2017, doi: 10.1016/j.isatra.2016.09.015.

[19] J. Qin, F. Léonard, and G. Abba, "Experimental external force estimation using a non-linear observer for 6 axes flexible-joint industrial manipulators," in *Proc. 2013 9th Asian Control Conf. (ASCC)*, Istanbul, Turkey, 2013, pp. 1–6, doi: 10.1109/ASCC.2013.6606364.

[20] S. Kružić, J. Musić, R. Kamnik, and V. Papić, "End-effector force and joint torque estimation of a 7-DoF robotic manipulator using deep learning," *Electronics*, vol. 10, no. 23, 2021, Art. no. 2963, doi: 10.3390/electronics10232963.

[21] O. Kaya et al., "Environmental force estimation for a robotic hand: Compliant contact detection," in *Proc. 2015 IEEE-RAS 15th Int. Conf. Humanoid Robots (Humanoids)*, Seoul, Korea (South), 2015, pp. 791–796, doi: 10.1109/Humanoids.2015.7363444.

[22] A. Alcocer et al., "Force estimation and control in robot manipulators," *IFAC Proc. Vol.*, vol. 36, no. 17, pp. 55–60, 2003.

[23] A. Colomé, D. Pardo, G. Alenyà, and C. Torras, "External force estimation during compliant robot manipulation," in *Proc. 2013 IEEE Int. Conf. Robot. Autom.*, Karlsruhe, Germany, 2013, pp. 3535–3540, doi: 10.1109/ICRA.2013.6631072.

[24] S. Liu, L. Wang, and X. V. Wang, "Sensorless force estimation for industrial robots using disturbance observer and neural learning of friction approximation," *Robot. Comp.-Integr. Manuf.*, vol. 71, 2021, Art. no. 102144.

[25] R. Loris and P. Dario, "Sensorless environment stiffness and interaction force estimation for impedance control tuning in robotized interaction tasks," *Auton. Robots*, vol. 45, pp. 371–388, 2021, doi: 10.1007/s10514-021-09970-z.

[26] T. Fujiki and K. Tahara, "Series admittance–impedance controller for more robust and stable extension of force control," *Robomech J.*, vol. 9, 2022, Art. no. 23, doi: 10.1186/s40648-022-00237-5.

[27] A. M. Abdullahi, A. Haruna, and R. Chaichaowarat, "Hybrid adaptive impedance and admittance control based on the sensorless estimation of interaction joint torque for exoskeletons: A case study of an upper limb rehabilitation robot," *J. Sens. Actuator Netw.*, vol. 13, no. 2, 2024, Art. no. 24.

Received: 26/03/2026; Revised: 20/04/2026; Accepted: 21/04/2026; Published: 25/04/2026